Friction **11**(7): 1225–1238 (2023)
https://doi.org/10.1007/s40544-022-0651-4
ISSN 2223-7690
CN 10-1237/TH
RESEARCH ARTICLE

Active control of friction realized by vibrational excitation: Numerical simulation based on the Prandtl–Tomlinson model and molecular dynamics

Xiao MA, Xinfeng TAN*, Dan GUO*, Shizhu WEN
State Key Laboratory of Tribology, Tsinghua University, Beijing 100084, China
Received: 04 December 2021 / Revised: 20 February 2022 / Accepted: 17 May 2022

Abstract: Superlubricity and active friction control have been extensively researched in order to reduce the consumption of fossil energy, the failure of moving parts, and the waste of materials. The vibration-induced superlubricity (VIS) presents a promising solution for friction reduction since it does not require high-standard environment. However, the mechanism underlying the VIS remains unclear since the atomic-scale information in a buried interface is unavailable to experimental methods. In this paper, the mechanism of VIS was examined via numerical calculation based on the Prandtl–Tomlinson (PT) model and molecular dynamics (MD) simulations. The results revealed that the pushing effect of stick–slip is one of the direct sources of friction reduction ability under vibrational excitation, which was affected by the response amplitude, frequency, and the trace of the tip. Moreover, the proportion of this pushing effect could be modulated by changing the phase difference when applying coupled vibrational excitation in *x*- and *z*-axis. This results in a significant change in friction reduction ability with phase. By this way, active friction control from the stick–slip to superlubricity can be achieved conveniently.

Keywords: superlubricity; vibration; friction control; molecular dynamics (MD)

1 Introduction

Friction, a ubiquitous natural phenomenon that affects daily life and industrial activities, presents significant challenges. Friction is responsible for about 23% of the total global energy consumption [1], as well as the failure of lots of parts. Although friction can be harmful to humans, it also has positive applications, such as braking, welding, and non-rigid connections. Extensive research has been conducted on active friction control and superlubricity. Various ways have been proposed to achieve superlubricity, such as structural superlubricity [2, 3] and liquid superlubricity [4, 5]. These methods have made great success and achieved superlubricity in the experimental environment. The vibration-induced superlubricity (VIS) is one of these methods that could achieve superlubricity and has broad prospects for industrial and micro-electro-mechanical system (MEMS) applications. Moreover, active friction control could be realized using the VIS under appropriate parameters.

Stick–slip is usually accompanied by mechanical instability and atomic vibration, representing the leading causes of energy dissipation at an atomic scale [6]. The first observation of the stick–slip phenomenon was reported by Mate et al. [7] when measuring the atomic friction between a tungsten tip and graphite substrate using the atomic force microscopy (AFM). The sawtooth-like modulation of the lateral force represents a typical feature of stick–slip [8]. When the tip is dragged over the periodic surface potential, it may stick to a low-energy point. When the pull force of the moving support is high enough to pull the tip from the current potential well, it slides until it becomes stuck in the following potential well. The

* Corresponding authors: Xinfeng TAN, E-mail: txf_1993@126.com; Dan GUO, E-mail: guodan26@tsinghua.edu.cn

instability of the motion caused by stick–slip leads to the dissipation of energy by phonon modes and electronic excitations [9, 10]. Moreover, the capacity of the dissipative channel affects the rate of dissipated energy [11–14].

The friction generated from stick–slip is directional, and it always obstructs the relative motion of friction pairs. If the current direction of relative motion is opposite to the main direction, the friction promotes the motion in the main direction at that moment. We name this phenomenon as the pushing effect of stick–slip, which is often disregarded due to the unavailability of the atomic-scale information within a buried interface using experimental methods. However, this effect may play a critical role in the measured friction during stick–slip. A typical instance is structural lubricity, showing that incommensurability can lead to relatively low friction [2, 3]. The molecular dynamics (MD) simulations provide more details about the buried interface of this phenomenon [15]. It shows that the stress distribution is homogeneous for the aligned system, while there is heterogeneous positive and negative alternation in misaligned systems. This heterogeneity suppresses the characteristic peaks of the overall friction and generates areas with negative friction [16, 17]. In typical experiments measuring atomic friction, the proportion of the pushing effect during the entire test process is small. However, this effect can be significantly increased using certain methods, consequently realizing active friction control. One of these technique applications is the VIS method.

Features of vibrational excitation that could effectively reduce friction were discovered and studied since 1960 [18–22]. The macroscopic vibrational excitation could reduce friction to a certain degree by changing the direction and magnitude of friction. Unlike the macroscale, one of the primary sources of friction at the nanoscale is derived from the stick–slip phenomenon, while vibrational excitation is also effective for friction reduction at this time. Socoliuc et al. [23] electrically excited the AFM tip in the normal direction while sliding over single crystals of NaCl and KBr. The friction and wear were reduced by the resulting variation in the interaction energy. Gnecco et al. [24] expanded this method to various materials and ambient environments by applying piezoelectric excitation instead of being limited to conductors and ultra-high vacuum (UHV). Besides normal vibration, Roth et al. [25] found that vibration along the sliding direction is also effective for reducing friction. Lantz et al. [26] showed that vibrational excitation significantly reduced the wear between the silicon tip and the polymer surface during long-distance sliding, significantly increasing the lifetime of parallel-probe storage systems. Pedraz et al. [27] found that normal vibration is able to reduce the wear-induced nanopatterning of polystyrene surface. Shi et al. [28] investigated the dependence of oscillation amplitude, frequency, and normal force on friction when normal vibrational excitation was applied. Cao and Li [29] introduced a piezoelectric thin film on the small-scale interface rather than additional vibration source or global excitation, which provided a convenient way for achieving active friction modulation.

Although the AFM experiments are helpful to reveal new insights about atomic friction, challenges arise in identifying the underlying mechanism of friction since the AFM does not provide detailed information regarding the buried interface. Numerical calculations based on the Prandtl–Tomlinson (PT) model and MD simulations can provide more information about this issue, presenting an excellent supplement to the AFM experiments involving atomic friction. Wang et al. [30] and Cheng et al. [31] studied the friction reduction ability of lateral (y-axis) and normal (z-axis) vibration on nanoscale using the PT model and MD simulations. However, further research for the mechanism of the friction reduction ability of vibrational excitation is still needed. In this paper, unidirectional vibration in all three axes and multi-directional vibration were studied using the PT model and MD simulations. According to these simulations, the pushing effect of stick–slip is one of the direct sources of the friction reduction ability of vibrational excitation. The proportion of this effect is affected by the response amplitude, frequency, and tip trace. Moreover, the motion state can be modulated from stick–slip to superlubricity by changing the phase difference under coupling excitation in x- and z-axis. This method provides a more convenient way to achieve active control of friction than unidirectional vibration excitation, which requires modulating the energy of excitation. Meanwhile, the x–z coupled

excitation could achieve stronger friction reduction ability than single direction excitation in *x*- or *z*-axis at the same energy level.

2 Models and methods

The numerical calculations based on the PT model were used for preliminary analysis. It has relatively fast calculation speeds and significant guidance for the actual experiments. In order to find appropriate parameters that can reduce friction and obtain a general understanding of the VIS, this method was used to simulate and analyze the VIS with a wide range of parameters. The PT model is a simple model, which involves a mass-spring oscillator sliding over the ideal potential energy surface (Fig. 1(a)). The motion of the oscillator is affected by the total potential energy, V, which consists of the elastic energy stored in the springs, V_{el}, and the interaction energy between the mass and the substrate, V_{int}. The expression of V is shown in Eq. (1) when vibrational excitation is applied in all three directions.

$$V(x,y)=-\frac{E_0\left(1+\alpha\sin\left(2\pi f_z t\right)\right)}{2}\cos\left(\frac{2\pi}{a}x\right)\cos\left(\frac{2\pi}{a}y\right)+\frac{1}{2}k_x\left(vt+\beta\sin\left(2\pi f_x t\right)-x\right)^2+\frac{1}{2}k_y\left(\gamma\sin\left(2\pi f_y t\right)-y\right)^2 \quad (1)$$

where α, β, and γ are the amplitudes of the vibrational excitation along the *z*-axis, the *x*-axis, and the *y*-axis, respectively, and f_z, f_x, and f_y represent the respective frequencies E_0 is the magnitude of the corrugation potential. The lattice constant is a = 5.4305 Å. The support moves along the *x*-axis at a speed, v, and the scanning time is t. The spring constant between the support and the mass point in the x and y direction is k_x and k_y, respectively.

The vibrator motion equation was obtained according to the total potential energy, as shown in Eqs. (2) and (3). The motion of the vibrator and the lateral force, F_L, during sliding were obtained by solving Eqs. (2) and (3).

$$m\ddot{x}+m\mu_x\dot{x}=-\frac{\pi E_0}{a}\left(1+\alpha\sin\left(2\pi f_z t\right)\right)\sin\left(\frac{2\pi x}{a}\right)\cos\left(\frac{2\pi y}{a}\right)+k_x\left(vt+\beta\sin\left(2\pi f_x t\right)-x\right)+\xi_x(t) \quad (2)$$

$$m\ddot{y}+m\mu_y\dot{y}=-\frac{\pi E_0}{a}\left(1+\alpha\sin\left(2\pi f_z t\right)\right)\cos\left(\frac{2\pi x}{a}\right)\sin\left(\frac{2\pi y}{a}\right)+k_y\left(\gamma\sin\left(2\pi f_y t\right)-y\right)+\xi_y(t) \quad (3)$$

where μ_x and μ_y are the damping coefficients of the *x*-direction and *y*-direction, respectively. $\xi_x(t)$ and $\xi_y(t)$ are the components of Gaussian distributed random noise along each direction. For convenience, we define

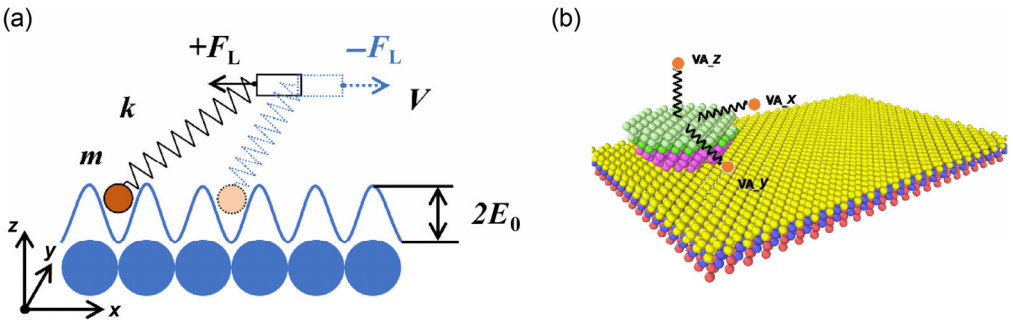

Fig. 1 Description of the PT model and MD model. (a) Schematic diagram of the PT model. The mass slides over the ideal potential energy surface dragged by the sliding support. A spring with stiffness, k, connects the mass, m, and the sliding support. Vibrational excitation in all three directions could be applied to the sliding support, which would drive the mass to vibrate at a certain frequency and response amplitude. The mass, spring, and the sliding support represented by the dotted lines show the situation when the pushing effect of stick–slip occurs. Negative lateral force is generated since the mass crosses the potential well in advance under the influence of vibration excitation. (b) MD simulation model. The radius of the hemispherical tip is 16 Å. The tip contains 443 silicon atoms, which are divided into three layers from the uppermost to lowermost, namely the rigid, thermostat, and Newton layers. The dimensions of the substrate are 130 Å × 87 Å × 9 Å. The substrate includes 5,376 silicon atoms, which are divided into three layers from the uppermost to the lowermost, namely the Newton, thermostat, and fixed layers.

the x-direction as the positive direction of friction, f, and F_L.

The pushing effect of stick–slip is shown in Fig. 1(a) represented by the dotted lines. Under the influence of vibrational excitation, the mass crosses the potential well much earlier. At this time, the movement distance of the mass may exceed the sliding support, which would change the spring from the extended state to the compressed state. Therefore, the direction of the lateral force changes from negative x-direction to positive x-direction, which is numerically negative at this time. Vibrational excitation increases the proportion of the pushing effect in the entire sliding process, so that the average friction is significantly reduced.

The PT model is an ideal model that has a lot of simplifications, which hinders the exploration for in-depth mechanism analysis. Compared with numerical simulation, MD simulation is more complex and precise. Therefore, the MD simulation is used to study the mechanism of friction reduction ability under specific parameters of the VIS. Although limited by computing power, MD simulation was not consistent with the actual experiment in terms of speed, mass, and some other parameters. However, it is still indicative to actual experiments. The MD simulation model is shown in Fig. 1(b). This model consists of a hemispherical silicon tip and silicon substrate. The radius of the tip is 16 Å, while the size of the substrate is 130 Å × 87 Å × 9 Å. The tip contains 443 silicon atoms and is divided into three layers: the rigid, thermostat, and Newton layers from the uppermost to the lowermost. The substrate contains 5,376 silicon atoms and is divided into three layers: Newton, thermostat, and fixed layers. The *NVE* ensemble is employed with the number of atoms, volume, and temperature conserved. The Langevin thermostat is used in the thermostat layers and absorbs heat from the adjacent Newton layer to maintain a constant temperature (0.1 K) of the system. The force of the atoms in the fixed layer is set to zero to eliminate the rigid motion of the substrate. Periodic boundary conditions are set in the x- and y-direction, while fixed boundary conditions are applied in the z-direction. The Tersoff potential [32] is used to describe the interaction between the silicon atoms in the tip and the substrate, while the Lennard–Jones (LJ) pair potential [33] delineated the interaction between them (with the parameters ε = 17.44 meV, σ = 0.3826 nm). Three virtual atoms are connected to the rigid layer via springs in all three directions, while the slide and vibration are transmitted to the tip through springs by controlling the displacement of virtual atoms directly. The spring stiffness is set to 2 N/m, while the load is 1 nN. The velocity of the virtual atom in the x-direction is 1 nm/ns. The vibrational frequency of virtual atoms ranges from 0 to 500 GHz, while the amplitude ranges from 0 to 20 Å in all three directions. The MD simulation package LAMMPS is used to carry out the MD simulations in this paper [34].

3 Single-direction vibrational excitation

The influence of vibrational excitation on the friction in all three directions was analyzed via numerical simulation based on the PT model at 0 K. Parameters of the PT model are set to be consistent with the MD model. The results are presented in Fig. 2 in a two-dimensional form. The friction mapping under y-axis excitation is not shown here since the friction characteristics are similar to those of the x-axis excitation. When the amplitude was less than 1 (the ratio between the drive amplitude and the potential amplitude for the z-direction excitation, and between the drive amplitude and the lattice constant for the x- or y-direction), an apparent frequency range for friction reduction appeared in the z-axis and x-axis, which corresponded to the prediction of Socoliuc et al. [23]. The friction decreased in all three directions as the vibration amplitude increased in this frequency range. Moreover, the excitation in the x- and y-axis improves the ability of the tip to cross the potential barrier, which leads to certain friction reduction ability at a low frequency and a large amplitude.

The friction reduction mechanism was analyzed in detail via the MD simulation. First, the frequency characteristics of the vibrational influence on friction reduction were evaluated via a frequency sweep with a fixed amplitude. Figure 3 shows the corresponding results. The drive amplitude was fixed at 20 Å for the z-axis excitation and 10 Å for the x- and y-axis excitation. Since the vibration in the z-direction was significantly affected by the interaction force between the tip and the substrate, the overall response amplitude is relatively low with a weak resonance peak. The

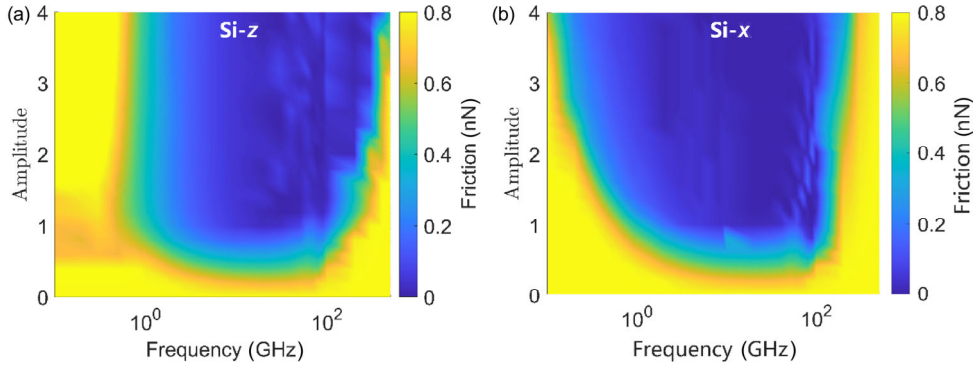

Fig. 2 Influence of vibrational excitation on friction (analyzed via numerical simulation). (a) Friction mapping under *z*-axis excitation. (b) Friction mapping under *x*-axis excitation. Friction mapping under *y*-axis excitation is not shown here since the friction characteristics have only slight differences with those of the *x*-axis excitation. The excitation frequency range in all three directions is 0.1–500 GHz, while the amplitude ratio range is 0–4. In the *z*-direction, the amplitude is the ratio of the potential energy amplitude, while it is the ratio of the lattice constant in the *x*- or *y*-direction.

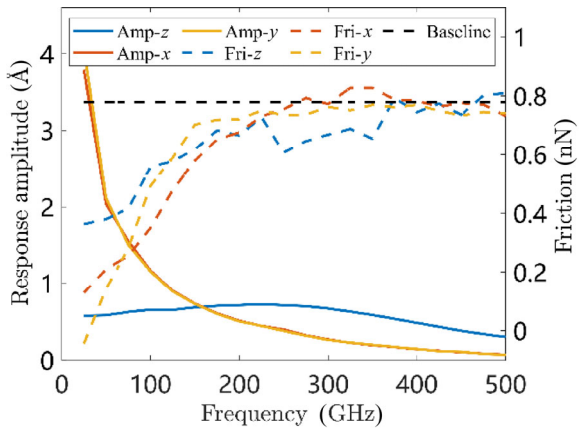

Fig. 3 Sweep frequency simulations of the vibrational excitation in all three directions (analyzed via the MD simulation). Simulations under vibrational excitation in different directions were expressed by different colors (the lines represented by blue, red, and yellow correspond to the excitation in *z*-axis, *x*-axis, and *y*-axis, respectively), while the solid and dashed lines represented the response amplitude and friction, respectively. The baseline is represented by a dashed black line, which expresses the friction simulated without vibrational excitation. The drive amplitude of the *z*-axis excitation was fixed at 20 Å, while those of the *x*- and *y*-direction were 10 Å. The drive frequency varies from 25 to 500 GHz.

friction under *z*-direction vibrational excitation (the dashed blue line) showed an overall upward trend. Compared with the friction without vibrational excitation (the dashed black line), the *z*-direction excitation reduced the friction by about 50% at low frequencies but lost its friction reduction ability at high frequencies. No resonance peaks were apparent for *x*- and *y*-direction in the plane, indicating that the forced oscillations in these two directions were overdamped. Moreover, the response amplitude and friction reduction ability gradually decreased as the frequency increased. The friction reduction ability of the excitation in the plane was more significant than that in the *z*-direction excitation at low frequencies but also disappeared at high frequencies. The friction slope of the *x*-axis excitation frequency (the dashed red line) was smaller than that of the *y*-direction excitation (the dashed yellow line), demonstrating that the friction reduction ability of *y*-axis vibration decreased faster as the frequency increased. This was primarily attributed to a coupling effect between the sliding and vibration, which existed in the *x*-direction but not in the *y*-direction.

Next, the origin of the friction reduction ability is analyzed in detail via the MD simulation. Figure 4 shows a comparison between the lateral force, the displacement in the *x*-direction, and the trace between experiments with and without excitation in the *z*-direction. Figure 4(a) suggests that the friction is significantly reduced under excitation in the *z*-direction. The average friction was 0.779 nN without vibrational excitation and 0.363 nN with the *z*-direction excitation (the amplitude and the frequency were 20 Å and 25 GHz, respectively). The peak force was significantly reduced under *z*-direction excitation, while the motion of the tip changed from multiple slips to single slip, as shown in Fig. 4(b). According to Fig. 4(b), the distance of a single stick–slip motion was sometimes even less than a lattice constant. Combined with

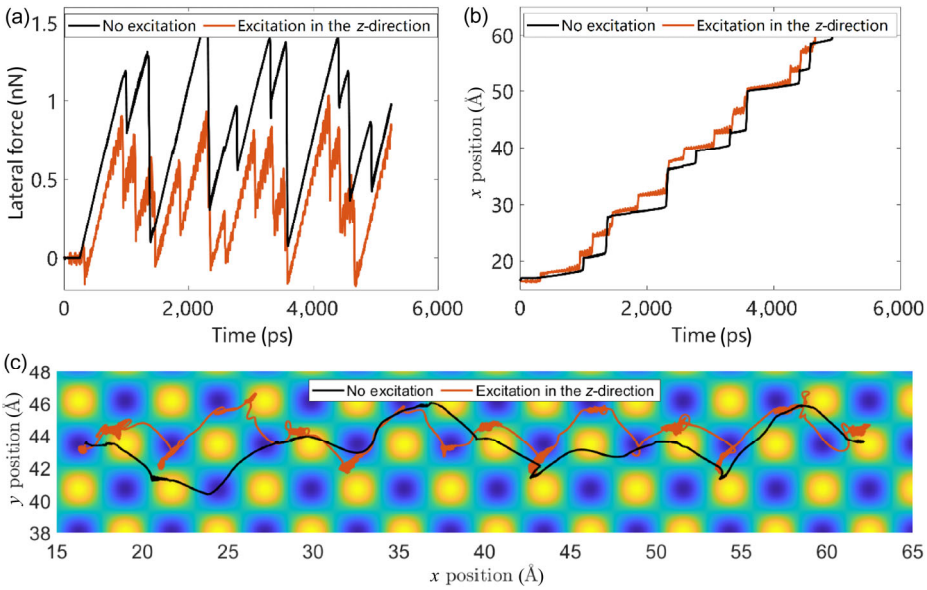

Fig. 4 Comparison between the simulations under no excitation and z-axis vibrational excitation via the MD simulation. The amplitude and frequency of z-axis excitation were 20 Å and 25 GHz, respectively. (a) Measured lateral forces during the simulation under no excitation and z-axis excitation. (b) Displacements of the tip centroid in the x-direction under no excitation and z-axis excitation. (c) Traces of the tip under no excitation and z-axis excitation.

Fig. 4(c), it can be inferred that the tip is more likely to bypass the potential barrier rather than cross it under excitation in the z-direction, rendering the average potential of this trace much lower than that of the trace without excitation. In addition, excitation in the z-direction slightly increased the height of the probe during the sliding process, weakening the interaction between the tip and the substrate.

Figure 5 compares the lateral forces, displacements, and traces between the experiments with and without excitation in the x-direction. The amplitude and frequency of x-axis excitation were 10 Å and 50 GHz, respectively. Unlike excitation in the z-direction, the stick–slip characteristics were not apparent under excitation in the x-direction, as shown in Fig. 5(a). Due to the relatively large response amplitude in the x-direction, the lateral force displayed positive and negative values in one cycle, rendering the average friction relatively small. The average friction is 0.779 nN when no excitation was applied and 0.210 nN when the x-direction excitation was applied. The weakening of the stick–slip characteristics is presented in Fig. 5(b). The tip displacement in the x-direction was generally ahead of the group without excitation. The ability of the tip to cross the barrier improved significantly with the assistance of x-direction excitation. Therefore, excitation in the x-direction rendered the path closer to a straight line, as shown in Fig. 5(c). It is worth mentioning that the absence of the stick–slip characteristics under x-direction excitation did not necessarily indicate the disappearance of the stick–slip phenomenon. Contrarily, only the stick–slip direction changed due to excitation in the x-direction. Therefore, at certain moments in a vibrational cycle, the lateral force was opposite to the instantaneous sliding direction but consistent with the overall sliding direction, denoting the pushing effect of stick–slip described above. The average friction was reduced significantly due to this phenomenon. However, active control of friction cannot be achieved easily with excitation in only one direction.

Figure 6 compares the lateral forces and displacements with and without excitation in the y-direction, and shows the trace of the tip under y-axis excitation. As shown in Fig. 6(a), the peak force at each stick period was reduced significantly. In addition, the friction reduction ability of y-direction excitation was displayed in the x-displacement, as shown in Fig. 6(b). The tip displacement under y-direction excitation kept ahead of the displacement without excitation. The average friction was 0.779 nN for the group without excitation and 0.142 nN for the experimental group

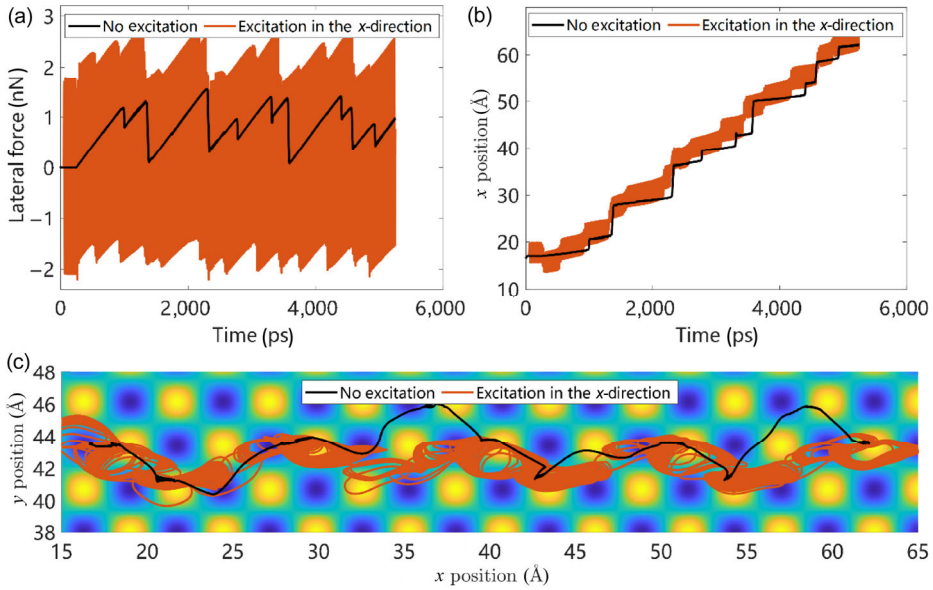

Fig. 5 Comparison between the simulations under no excitation and *x*-axis vibrational excitation via the MD simulation. The amplitude and frequency of *x*-axis excitation were 10 Å and 50 GHz, respectively. (a) Measured lateral forces during the simulation under no excitation and *x*-axis excitation. (b) Displacements of the tip centroid in the *x*-direction under no excitation and *x*-axis excitation. (c) Traces of the tip under no excitation and *x*-axis excitation.

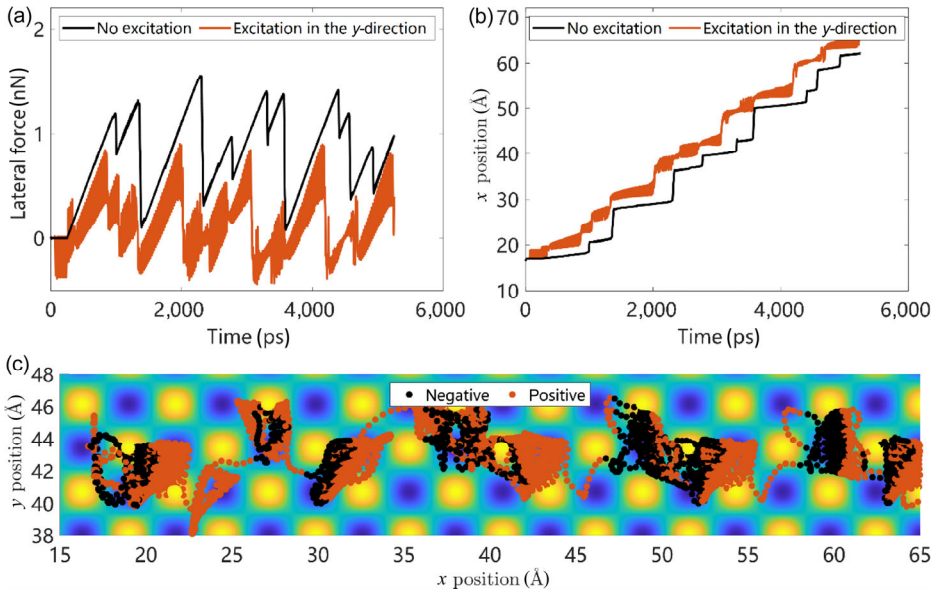

Fig. 6 Comparison between the simulations under no excitation and *y*-axis vibrational excitation via the MD simulation. The amplitude and frequency of the *y*-axis excitation were 10 Å and 50 GHz, respectively. (a) Measured lateral forces during the simulation under no excitation and *y*-axis excitation. (b) Tip displacements in the *x*-direction under no excitation and *y*-axis excitation. (c) Traces of the tip centroid under *y*-axis excitation. The black point indicates that the lateral force was negative at this point, while the red point indicates positive lateral force.

with excitation in the *y*-direction. The trace of the tip under *y*-direction excitation is shown in Fig. 6(c). Due to vibrational excitation in the *y*-direction, the tip crossed the potential barrier laterally to generate an instantaneous movement under the influence of the adjacent potential barrier, which was opposite to the sliding direction. This resulted in a period of negative lateral force. The pushing effect of stick–slip excited by lateral movement was the main source for the friction reduction ability of excitation in the *y*-direction.

According to the numerical simulation based on the PT model, unidirectional vibrational excitation has good friction reduction ability in all three directions. This ability exists in an appropriate frequency range and increases significantly as the amplitude rises. The mechanism of the friction reduction ability of vibrational excitation in all three directions is analyzed through the MD simulation. The excitation frequency has little effect on the response amplitude in the z-direction, but it would change the trace of the tip. The tip is more likely to bypass the potential barrier rather than cross it under the excitation in z-direction. The average potential of the trace under z-direction excitation is much lower than that of the trace without excitation, rendering much lower average friction. The excitation frequency has a greater influence on the response amplitude in the x- and y-direction. The response amplitude is very large at the appropriate frequency, which enhances the ability to cross the potential barrier along x- or y-direction. The pushing effect is stimulated at this time, so that the average friction is reduced.

Moreover, we did some preliminary research about the VIS method using the PT model. These time parameters consistent with the MD simulation were not chosen since the vibrational frequency was too high to keep low energy consumption. The range of frequency is 0 to 1×10^7 Hz, while the range of amplitude is 0 to 2 times of the lattice constant. The sliding speed is 1 nm/s, while the mass is 1×10^{-12} kg. Figure 7(a) shows the distribution of friction under this set of parameters, while Fig. 7(b) shows the energy consumption distribution. The energy dissipation for sliding over each lattice constant is 5 eV when no excitation was applied. Since the energy dissipation increases exponentially with the increase of vibrational frequency and amplitude, the maximum value of the color bar in Fig. 7(b) is set to 10 eV for a better resolution. Comparing the distributions of friction and energy, it is obvious that there is a parameter range that can effectively reduce the friction without significantly increased energy. Although the VIS method does not seem to have advantage in reducing energy dissipation, it is still possible to obtain significant friction reduction with less energy input.

4 Multi-directional vibrational excitation coupling

Section 3 shows the friction reduction ability when uniaxial vibrational excitation is applied. Realizing the active control of friction in this mode requires changing the excitation amplitude and frequency, which is inefficient and unstable. However, the active control of friction can be realized in a simple way under multi-directional vibrational excitation. Figure 8 shows the friction reduction ability under multi-directional excitations simulated using numerical methods, where Figs. 8(a)–8(c) represent the x–z, y–z, and x–y couplings, respectively. The friction changed significantly with the phase difference under x–z coupled excitation, while this effect was not significant in the other two combinations. In addition, the friction under x–z coupled excitation exhibited a 2π cycle. To examine the mechanism underlying this effect and realize active friction control, a more in-depth investigation was performed via the MD simulation.

The friction reduction ability under x–z coupled excitation was analyzed in detail via the MD simulation. The friction varied with the z-axis excitation phase,

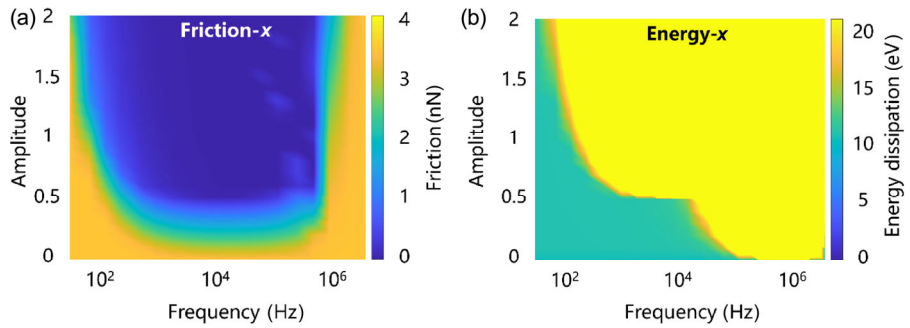

Fig. 7 Research on energy consumption of the VIS. (a) Friction distribution when x-axis vibrational excitation was applied; (b) energy dissipation distribution when x-axis vibrational excitation was applied.

as shown in Fig. 9(a). The amplitudes of the two uniaxial excitations were 4 Å for the *x*-axis and 10 Å for the *z*-axis. The coupled two excitations vibrated at the same frequency (25, 50, or 75 GHz). The *x*-axis excitation displayed a fixed phase, while that of the *z*-axis excitation varied from 0 to 2π. Although the uniaxial excitation of these two sets of parameters exhibited apparent friction reduction ability, superlubricity could not be reached. However, the friction reduction ability changed with the phase when coupling the two uniaxial excitations. Of the three coupled frequencies, *x*–*z* coupled excitation at 25 GHz demonstrated the strongest friction control ability. When the phase was zero, the friction was close to zero, even reaching a negative value. When the phase was π, the friction reached the maximum value, close to 0.6192 nN, which exceeded the values when the two uniaxial excitations were applied alone. Furthermore, *x*–*z* coupled excitation at 25 GHz realized friction control from −0.0125 to 0.6192 nN. These values were 0.0552 to 0.6176 nN and 0.1491 to 0.488 nN for coupled excitation at 50 and 75 GHz, respectively. The friction control ability gradually decreased with an increase in excitation frequency. For the *x*–*z* coupled excitation at 25 GHz, another set of simulation was performed with only the sliding direction reversed, as shown in Fig. 9(a) by the purple dashed line. When the sliding direction is reversed, the phenomenon related to the phase of *x*–*z* coupled excitation is exactly differing by π. The mechanism of this phenomenon will be discussed in this section later.

Although the response amplitude is one of the most critical factors affecting friction during uniaxial excitation, it does not cause changes in friction during dual-axis coupled excitation. As shown in Fig. 9(b), the dashed line with triangle marks, the dashed line with "×" marks, and the solid blue line represent the response amplitudes in the *z*-axis, the *x*-axis, and the friction, respectively. The response amplitude fluctuated slightly in a specific range in the *z*-direction. Contrarily, the response amplitude in the *x*-direction gradually increased with an increase in friction. In addition, the height data indicated that the tip position was higher at phase zero than that at phase π. Therefore, the tip was usually at the bottom of the

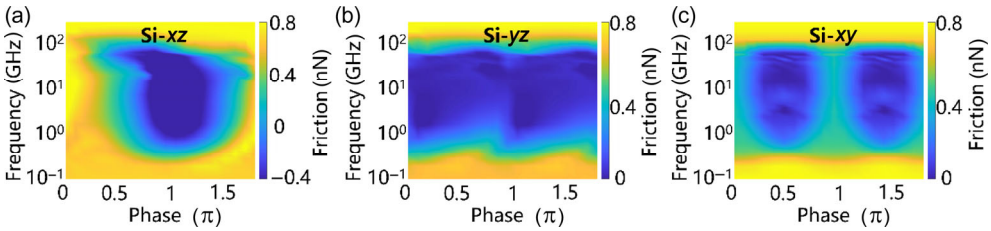

Fig. 8 Variations in the friction with phase and frequency under bidirectional excitation via numerical simulation based on the PT model. The parameters of the PT model are set to be consistent with the MD model. (a) *x*–*z* bidirectional excitation; (b) *y*–*z* bidirectional excitation; and (c) *x*–*y* bidirectional excitation.

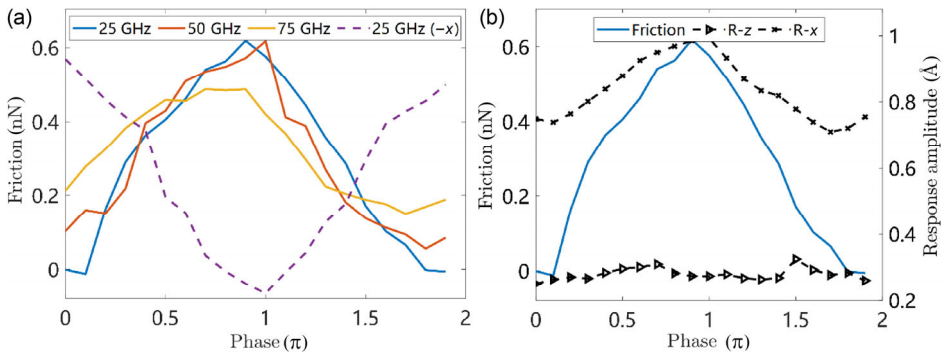

Fig. 9 The friction reduction ability of *x*–*z* coupled excitation. (a) Variations in the friction with the phase difference under the *x*–*z* coupled excitation at different frequencies. The blue, red, and yellow solid lines represent the *x*–*z* coupled excitation at 25, 50, and 75 GHz, respectively. The purple dashed line represents the *x*–*z* coupled excitation at 25 GHz with reverse sliding direction. (b) Variations in the frictional force and response amplitude with the phase difference under the *x*–*z* coupled excitation at 25 GHz.

potential well at phase π, while reaching a higher potential position at phase zero. The difference in the energy of the position led to variation in the response amplitude. However, an increase in the response amplitude in this situation did not enhance the friction reduction ability as in the case of uniaxial excitation, since the response vibration at this time failed to cross the energy barrier.

Figure 10 shows the traces of the tip at phase zero and phase π. The colors of the data points are consistent with those in Fig. 6. Negative lateral force accounted for more than half of the force data measured at phase zero, reaching 50.65%. This indicates that the pushing effect of stick–slip widely exists under *x*–*z* coupled excitation at phase zero. Contrarily, negative lateral force accounted for less than 20% at phase π. This shows that the proportion of the pushing effect can be adjusted specifically, such as the phase difference under *x*–*y* coupled excitation.

Therefore, the phase difference caused such a substantial change in friction under *x*–*z* coupled excitation. This could be attributed to the fact that the phase difference changed the vibration shape when two directional excitations were coupled. Figure 11 shows the vibration diagram at phases zero and π under *x*–*z* coupled excitation. The inset represents the theoretical vibration diagram and the potential energy surface, while the main graph represents the displacement of the tip in the *x*–*z* plane. Consequently, the actual vibration shape of the tip is close to the theoretical vibration shape. This suggests that the vibration shape significantly affected the sliding friction, while the phase difference changed the vibration shape of the *x*–*z* coupled excitation. The vibration shape changed the friction by aiding the tip to cross the energy barrier. When the tip moved forward to cross the potential barrier, the vibration direction was nearly parallel to the tangent of the potential energy surface at phase zero. The tip reached a peak in the *x*- and *z*-direction simultaneously. Therefore, the vibration aided the tip in crossing the energy barrier. However, at phase π, the vibration shape was almost perpendicular to the tangent of the potential energy surface. When the tip reached the peak in the *x*-direction, it was also in the trough in the *z*-direction. Consequently, the vibration failed to assist the tip in crossing the energy barrier and hindered this process. The phenomenon obtained after reversing the sliding direction in Fig. 9(a) provides strong support for this mechanism.

As mentioned before, bidirectional *x*–*z* coupled excitation displays a powerful friction control ability. However, whether bidirectional vibrational excitation

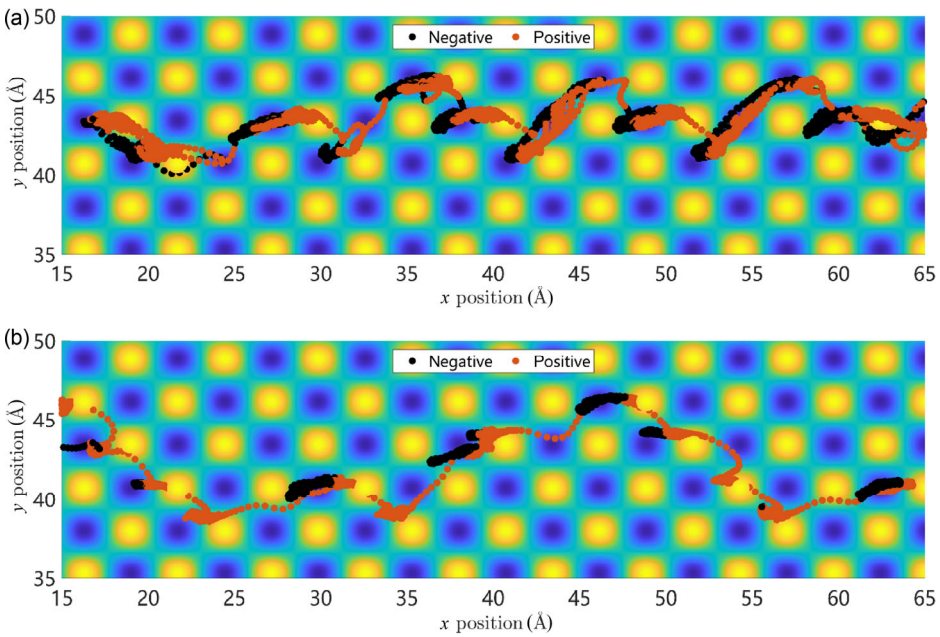

Fig. 10 Traces of the tip at 25 GHz *x*–*z* coupled excitation at (a) phase zero and (b) phase π (via the MD simulation). The colors of the trace are determined according to the sign of the friction at that moment. The black points indicate negative lateral force, while the red points denote positive lateral force.

is more effective in friction reduction compared to uniaxial vibrational excitation or not requires further examination. Therefore, the friction was measured at different phases by fixing the total input energy and changing the proportion of vibrational energy in the x-direction, as shown in Fig. 12. At phase zero or 0.25 π, the friction initially decreased to zero in conjunction with an energy increase in the x-direction, after which it gradually rose to the friction of uniaxial excitation in the x-direction. At phase 0.5π, the friction gradually decreased with increased energy in the x-direction. Regardless of the energy changes, the friction at phase 0.5π was almost always larger than the friction when x-axis excitation was applied alone ($E_x/E_{\text{total}} = 1$). At phases 0.75π and π, the friction

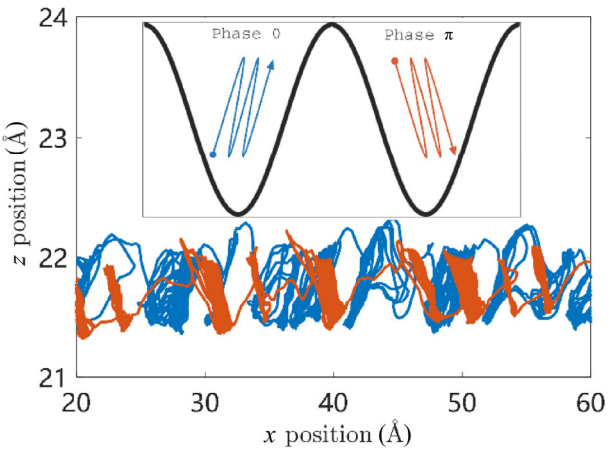

Fig. 11 Prediction (the inset) and simulation of the vibrational shape under x–z coupled excitation. The solid blue lines represent the vibration shape at phase zero, while the solid orange lines represent the vibration shape at phase π.

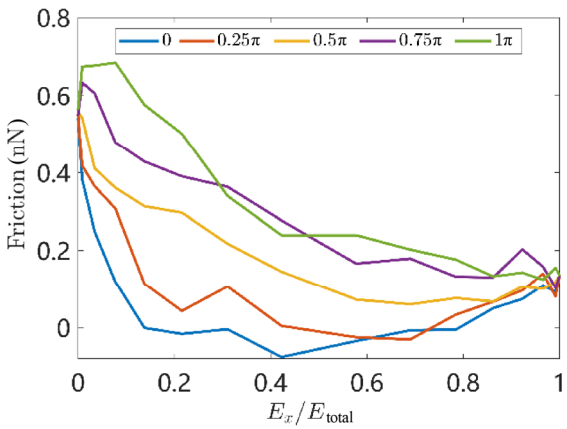

Fig. 12 Variations of average friction under x–z coupled excitation with the energy in the x-direction, E_x, changing while the total energy, E_{total}, kept constant.

increased first, followed by a gradual decrease in conjunction with a rise in energy in the x-direction. In summary, x–z coupled excitation displayed a stronger friction reduction ability at about phase zero than unidirectional vibrational excitation, while the energy ratio of 0.5 was necessary to achieve superlubricity. However, x–z coupled excitation no longer exhibited stronger friction reduction ability than unidirectional vibrational excitation when the phase increased. Moreover, x–z coupled excitation achieved significantly higher friction in a specific proportion range at phase π.

5 Conclusions

Atomic friction typically originates from mechanical instability and lattice vibration due to stick–slip motion. Although the proportion is small, negative lateral force is evident in atomic friction, named as the pushing effect of stick–slip, which is often ignored due to the unavailability of the atomic-scale information within a buried interface when using experimental methods. However, this information can be obtained via simulation. This article examines the impact of vibrational excitation on atomic friction via the numerical and MD simulations. We found that the pushing effect is one of the direct sources for the friction reduction ability of the VIS method. The proportion of pushing effect in atomic friction increases significantly via unidirectional vibrational excitation, leading to ultra-low friction. The proportion of this effect was affected by the response amplitude, frequency, and trace of the tip. Furthermore, a stronger friction reduction ability can be achieved through multi-directional vibrational excitation coupling, especially for coupled excitation in x- and z-axis. Active atomic friction control can be attained in this way by changing the phase difference between excitation in these two directions, which modulates the atomic friction from stick–slip to superlubricity.

Acknowledgements

This research is financially supported by the National Natural Science Foundation of China (Grant Nos. 52175175 and 51527901).

References

[1] Holmberg K, Erdemir A. Influence of tribology on global energy consumption, costs and emissions. *Friction* **5**(3): 263–284 (2017)

[2] Hirano M, Shinjo K, Kaneko R, Murata Y. Anisotropy of frictional forces in muscovite mica. *Phys Rev Lett* **67**(19): 2642–2645 (1991)

[3] Dienwiebel M, Verhoeven G S, Pradeep N, Frenken J W, Heimberg J A, Zandbergen H W. Superlubricity of graphite. *Phys Rev Lett* **92**(12): 126101 (2004)

[4] Raviv U, Giasson S, Kampf N, Gohy J F, Jérôme R, Klein J. Lubrication by charged polymers. *Nature* **425**(6954): 163–165 (2003)

[5] Li J J, Liu Y H, Luo J B, Liu P X, Zhang C H. Excellent lubricating behavior of *Brasenia schreberi* mucilage. *Langmuir* **28**(20): 7797–7802 (2012)

[6] Hu Y Z, Ma T B, Wang H. Energy dissipation in atomic-scale friction. *Friction* **1**(1): 24–40 (2013)

[7] Mate C M, McClelland G M, Erlandsson R, Chiang S. Atomic-scale friction of a tungsten tip on a graphite surface. In: *Scanning Tunneling Microscopy*. Neddermeyer H, Ed. Dordrecht (the Netherlands): Springer Dordrecht, 1987: 226–229.

[8] Socoliuc A, Bennewitz R, Gnecco E, Meyer E. Transition from stick–slip to continuous sliding in atomic friction: Entering a new regime of ultralow friction. *Phys Rev Lett* **92**(13): 134301 (2004)

[9] Li B, Clapp P C, Rifkin J A, Zhang X M. Molecular dynamics simulation of stick–slip. *J Appl Phys* **90**(6): 3090–3094 (2001)

[10] Johnson K L, Woodhouse J. Stick–slip motion in the atomic force microscope. *Tribol Lett* **5**(2–3): 155–160 (1998)

[11] Park J Y, Ogletree D F, Thiel P A, Salmeron M. Electronic control of friction in silicon pn junctions. *Science* **313**(5784): 186 (2006)

[12] Filleter T, McChesney J L, Bostwick A, Rotenberg E, Emtsev K V, Seyller T, Horn K, Bennewitz R. Friction and dissipation in epitaxial graphene films. *Phys Rev Lett* **102**(8): 086102 (2009)

[13] Wada N, Ishikawa M, Shiga T, Shiomi J, Suzuki M, Miura K. Superlubrication by phonon confinement. *Phys Rev B* **97**(16): 161403 (2018)

[14] Cannara R J, Brukman M J, Cimatu K, Sumant A V, Baldelli S, Carpick R W. Nanoscale friction varied by isotopic shifting of surface vibrational frequencies. *Science* **318**(5851): 780–783 (2007)

[15] Dong Y, Li Q, Wu J, Martini A. Friction, slip and structural inhomogeneity of the buried interface. *Modelling Simul Mater Sci Eng* **19**(6): 065003 (2011)

[16] Zhu P Z, Li R. Study of nanoscale friction behaviors of graphene on gold substrates using molecular dynamics. *Nanoscale Res Lett* **13**(1): 34 (2018)

[17] Dong Y, Wu X, Martini A. Atomic roughness enhanced friction on hydrogenated graphene. *Nanotechnology* **24**(37): 375701 (2013)

[18] Pohlman R, Lehfeldt E. Influence of ultrasonic vibration on metallic friction. *Ultrasonics* **4**(4): 178–185 (1966)

[19] Lenkiewicz W. The sliding friction process—Effect of external vibrations. *Wear* **13**(2): 99–108 (1969)

[20] Choi K S, Graham M. Drag reduction of turbulent pipe flows by circular-wall oscillation. *Phys Fluids* **10**(1): 7–9 (1998)

[21] Gee R, Hanley C, Hussain R, Canuel L, Martínez J. Axial oscillation tools vs. lateral vibration tools for friction reduction—What's the best way to shake the pipe? In: Proceedings of the SPE/IADC Drilling Conference and Exhibition, London, UK, 2015: SPE-173024-MS.

[22] Popov M, Popov V L, Popov N V. Reduction of friction by normal oscillations. I. Influence of contact stiffness. *Friction* **5**(1): 45–55 (2017)

[23] Socoliuc A, Gnecco E, Maier S, Pfeiffer O, Baratoff A, Bennewitz R, Meyer E. Atomic-scale control of friction by actuation of nanometer-sized contacts. *Science* **313**(5784): 207–210 (2006)

[24] Gnecco E, Socoliuc A, Maier S, Gessler J, Glatzel T, Baratoff A, Meyer E. Dynamic superlubricity on insulating

and conductive surfaces in ultra-high vacuum and ambient environment. *Nanotechnology* **20**(2): 025501 (2009)

[25] Roth R, Fajardo O Y, Mazo J J, Meyer E, Gnecco E. Lateral vibration effects in atomic-scale friction. *Appl Phys Lett* **104**(8): 083103 (2014)

[26] Lantz M A, Wiesmann D, Gotsmann B. Dynamic superlubricity and the elimination of wear on the nanoscale. *Nat Nanotechnol* **4**(9): 586–591 (2009)

[27] Pedraz P, Wannemacher R, Gnecco E. Controlled suppression of wear on the nanoscale by ultrasonic vibrations. *ACS Nano* **9**(9): 8859–8868 (2015)

[28] Shi S, Guo D, Luo J B. Micro/atomic-scale vibration induced superlubricity. *Friction* **9**(5): 1163–1174 (2021)

[29] Cao J W, Li Q Y. Vibration-induced nanoscale friction modulation on piezoelectric materials. *Friction* **10**(10): 1650–1659 (2022)

[30] Wang Z N, Duan Z Q, Dong Y, Zhang Y. Molecular dynamics simulation of lateral ultrasonic excitation in atomic-scale friction. *Mater Res Express* **7**(1): 015089 (2020)

[31] Cheng Y, Zhu P Z, Li R. The influence of vertical vibration on nanoscale friction: A molecular dynamics simulation study. *Crystals* **8**(3): 129 (2018)

[32] Tersoff J. Modeling solid-state chemistry: Interatomic potentials for multicomponent systems. *Phys Rev B* **39**(8): 5566–5568 (1989)

[33] Agrawal P M, Raff L M, Komanduri R. Monte Carlo simulations of void-nucleated melting of silicon via modification in the Tersoff potential parameters. *Phys Rev B* **72**(12): 125206 (2005)

[34] Plimpton S. Fast parallel algorithms for short-range molecular dynamics. *J Comput Phys* **117**(1): 1–19 (1995)

Xiao MA. He obtained his B.S. degree in mechanical engineering from Tsinghua University, Beijing, China, in 2017. Currently, he is a Ph.D. candidate in the State Key Laboratory of Tribology at Tsinghua University, Beijing, China. His research focuses on vibration induced superlubricity and active friction control in micro/nanoscale.

Xinfeng TAN. He obtained his B.E. degree from Beihang University, China, in 2015, and received his Ph.D. degree in mechanical engineering in 2020 from Tsinghua University, China. He is working at State Key Laboratory of Tribology, Tsinghua University for postdoctoral research. His research interests include the dynamic friction energy dissipation detection at micro-nano scale as well as the design and improvement of micro-nano tribometer based on atomic force microscope.

Dan GUO. She received her M.S. degree in engineering mechanics in 1995 from Xi'an Jiaotong University, Xi'an, China, and her Ph.D. degree in engineering mechanics in 1999 from Tsinghua University, Beijing, China. She joined the State Key Laboratory of Tribology at Tsinghua University, Beijing, China, from 1999. Her current position is a professor and the deputy director of the laboratory. Her research areas cover the properties of friction at the micro/nanoscale, mechanism of interaction among nanoparticles and surface in ultra-smooth surface planarization, and the formation and failure of lubricant film in harsh conditions.

Shizhu WEN. He received his B.E. degree in the Department of Precision Instruments and Mechanology, Tsinghua University, Beijing, China, in 1955. He went to Imperial College London, London, UK, as a visiting scholar between 1979 and 1981. He is an academician of the Chinese Academy of Sciences and the honorary director of State Key Laboratory of Tribology at Tsinghua University, Beijing, China. He had received 19 national or ministerial prizes for his distinguished research achievements, including the second prize in the National Natural Science Awards, the third prize in the National Technology Invention Awards, 2004 award for Teaching & Research of Tsinghua University, and the Science and Technology Achievement Award of the Ho LEUNG and Ho LEE Foundation in 2002. His research interests are elastohydrodynamic lubrication, thin-film lubrication, the mechanism of friction control and wear, nanotribology, and micro-machine design.